Geoderma 438 (2023) 116650

Contents lists available at ScienceDirect

Geoderma

journal homepage: www.elsevier.com/locate/geoderma

Water-dispersible colloids distribution along an alluvial fan transect in hyper-arid Atacama Desert

Xiaolei Sun [a,b,*], Simon Matthias May [c], Wulf Amelung [a,d], Ni Tang [a,b], Dominik Brill [c], Franko Arenas-Díaz [e], Daniel Contreras [f], Bárbara Fuentes [f], Roland Bol [a,g], Erwin Klumpp [a]

[a] Institute of Bio- and Geosciences, Agrosphere (IBG-3), Forschungszentrum Jülich, 52425 Jülich, Germany
[b] Institute for Environmental Research, Biology 5, RWTH Aachen University, Worringerweg 1, 52074 Aachen, Germany
[c] Institute of Geography, University Cologne, Albertus-Magnus-Platz, 50923 Cologne, Germany
[d] Institute of Crop Science and Resource Conservation, Soil Science and Soil Ecology, University of Bonn, Nussallee 13, 53115 Bonn, Germany
[e] Programa de Doctorado en Ciencias mención Geología, Universidad Católica del Norte, Antofagasta, Chile
[f] Departamento de Ingeniería Química, Universidad Católica del Norte, Antofagasta, Chile
[g] School of Natural Sciences, Environment Centre Wales, Bangor University, Bangor, United Kingdom

ARTICLE INFO

Handling Editor: M. Tighe

Keywords:
Flow field-flow fractionation
Topographic variations
Atmospheric deposition
Aeolian work
Leaching process

ABSTRACT

As located in one of the oldest and driest deserts on Earth, soils in the Atacama Desert are greatly affected by atmospheric dust deposited on soil surface and the related fate of water-dispersible colloids (WDCs, <300 nm). We hypothesize that formation and content of these WDCs change with topography and age of natural soils. To highlight the processes involved, we investigated a mid-sized and gently (~5°) sloping alluvial fan system of multi-phase evolution at 1480 m a.s.l. in the Paposo region of the hyper-arid Atacama Desert, which is considered typical for this part of the Coastal Cordillera. Sampling was done along a topographic transect in 11 pits, and assessed the distribution and composition of WDCs by means of asymmetric flow field-flow fractionation (AF4). The younger fan section (optically stimulated luminescence (OSL)-age of ~13.6 ka) exhibited a pronounced surface roughness and steep slopes. Here, WDCs from the top soils (0–1 cm) free of plants contained nearly 54 ± 7% of medium-sized colloids (MCs, 210–300 nm) with a dominance of Si and Al. The elevated concentrations of fine colloids (FC, 24–210 nm) and particularly nanocolloids (NCs, 0.6–24 nm) was shown in levelled surface soils near shrubs with predominance of organic carbon (OC) and Ca. With higher collodial OC and Ca content in soils near shrubs, more WDC-P was formed concomitantly through increased OC-Ca-P associations. Larger variations in total WDC content were detected in the surface soils of the older fan section, which was dated to ~56.4 ka. Here, the peaking NC had almost disappeared and thus MC dominated, probably reflecting re-aggregation and wind erosion over longer periods of time across a relatively smooth land surface. The WDCs and WDC-P peaked at 5–10 cm depth in the older fan section, as here a solid mineral/salt layer was present, while in the younger fan section the WDCs were more likely to be translocated from 'permeable' surface into deeper layers, likely reflecting leaching with occasional heavy rainfall. Overall, forms and distribution of WDCs depended on both topographic position and sediment age, thus making colloids as unique tracers of soil development processes during myriad or more years.

1. Introduction

It has been suggested that soil formation and properties in the Atacama Desert are affected largely by the atmospheric deposition of particulate material on soils (Ewing et al., 2006; Wang et al., 2014; Li et al., 2019). Amundson et al. (2012) found that a volume of 50% or more of particles came from atmospheric deposition. As one of the oldest and driest deserts on Earth, most areas of the Atacama Desert have experienced long-term hyper-arid conditions with limited water availability (Davis et al., 2014; Sáez et al., 2012; Sun et al., 2018). These special climatic conditions make it possible to preserve the sedimentary record because of the very low (usually water-driven) erosion rates and leaching processes (Arenas-Díaz et al., 2022). The prevailing topographic conditions, such as the natural barrier of cordilleras preventing

* Corresponding author at: Institute of Bio- and Geosciences, Agrosphere (IBG-3), Forschungszentrum Jülich, 52425 Jülich, Germany.
E-mail address: xi.sun@fz-juelich.de (X. Sun).

https://doi.org/10.1016/j.geoderma.2023.116650
Received 15 December 2022; Received in revised form 18 August 2023; Accepted 22 August 2023
Available online 31 August 2023

dust outbreaks, reduce aeolian entrainment and wind reworking, which also contribute to the preservation of fine-grained deposits in the pedosphere (Carretier et al., 2018; Placzek et al., 2010; Reyers et al., 2019).

However, dust deposited in soils differs in particle size, shape, composition, and mineralogic properties due to variations in sources, transportation processes, and aeolian transformation (Choobari et al., 2014; Reyers et al., 2019). In addition, fine particles in the atmosphere are difficult to immobilize due to the smooth surface of desert pavements, which may be prone to wind erosion (Clarke, 2006). Because of insufficient humidity to support plant growth or microbial activities in the hyper-arid region, organic carbon (OC) contents and nutrient (like phosphorus) turnover are low (Ewing et al., 2006; Mörchen et al., 2019; Latorre et al., 2003). These uncertainties during the soil formation processes make it difficult to identify element accumulation and nutrient cycling in the hyper-arid region, especially in areas where there is a lack of wet deposition combined with less fog penetration.

Soil colloids with common particle size of 1–10^3 nm are characterized by high specific surface areas with a large bonding capacity for mineral elements (e.g., Si, Al, Fe, Ca, and Mg) and nutrients such as phosphorus (P) and OC (Missong et al., 2018a; Zhang et al., 2021). As the smallest particulate phase in soils, these colloids are sensitive to disturbances in pedogenesis, which can increase the transformation and transport of both mineral elements and nutrients (Missong et al., 2018b). P is one of the limited nutrients for life and it shows high mobility in soil systems along with colloid particles by bonding to organic or mineral fractions (Bol et al., 2018; Wang et al., 2020). In water-limited regions like desert or neighboring margins, the aeolian deposition of P is one of the pathways for the long-term maintenance of productivity (Okin et al., 2004). In the Atacama Desert, dust-born P additions may have a local reach as the dust cycle here is isolated from the global scale (Arenas-Díaz et al., 2022; Ginoux et al., 2012). Furthermore, occasional rainfall enhances the life bloom which may result in the accumulation of P in soils by exchanging dominant size particles or bonding ways. The varied bonding forms among different colloidal sizes may not only affect the P availability but also reflect the state of fine particle aggregations (Jiang et al., 2015b; Zhang et al., 2021). However, past studies have mainly focused on the dynamics of colloids and the availability and bonding forms of colloidal-P in organic-rich soils such as forest, agricultural land, or grassland soils (Jiang et al., 2015a; Li et al., 2021; Missong et al., 2018b). Only a few studies have investigated colloids in a landscape free of vegetation, such as in the central Atacama Desert.

In a preliminary study by Moradi et al. (2020), the depth distribution of the water-dispersible colloids (WDCs, <500 nm) and P content from each 10 cm was investigated in the active ("Fan") and abandoned ("Crust") sections of an alluvial fan system in a hyper-arid region of the Atacama Desert. The results showed that the movement and distribution of colloids were affected by small, local scale differences, as the crust-like surface may have been beneficial for nanoparticle accumulation due to reduced infiltration capacity during water leaching processes. However, only two sites were sampled and analyzed in the study, which provided limited information about the alluvial system. In general, alluvial fans are typical landforms that provide geomorphic surfaces with a multiphase history of soil formation (Bartz et al., 2020). Alluvial fan formation usually occurs during the multiple wetter periods before the late Pliocene (Amundson et al., 2012). Subsequently, during long-term dryer periods, wind erosion and dust accumulation tended to smooth the surface and form mature desert pavements in alluvial fan systems with limited runoff and an absence of vegetation (Carretier et al., 2018). Though fluvial impacts on the landscape have been extremely rare in recent centuries, several remarkable rainfall events driven by the El Niño–Southern Oscillation (ENSO) were recorded in the past three decades, including in June 1991, February 2001, March 2015, and June 2017 (Houston, 2006; Jordan et al., 2020; Ortega et al., 2019; Reyers et al., 2021; Schween et al., 2020). These occasional rainfalls may have facilitated plant growth, resulting in the transformation of nutrients like P (Jordan et al., 2020; Orlando et al., 2010). In addition, infiltration processes that remove fine materials from the surface to deeper layers are easily triggered by the high permeability that is characteristic of the salt-rich soils in the Atacama Desert (Aguilar et al., 2020; Jungers et al., 2013; Pfeiffer et al., 2021). Therefore, not only the morphological features, but also the topographic variations, the age of the soil parent material, and plant growth in an alluvial fan system may all be of relevance with regard to the turnover of fine colloids in soils. Here, a new transect of 11 pits along the same alluvial fan system studied by Moradi et al. (2020) was sampled in order to provide more details on WDC and colloidal-P distribution in relation to the different alluvial fan sections. For the lower to intermediate elevations of the steep Coastal Cordillera in this part of the Atacama Desert, mid-sized alluvial fans with surface slopes of 5–6° and at least two different surface generations such as the one investigated here are typically found at the transition of smaller streams to the episodically active and broad channels of the larger Quebradas. In addition, subdivision sampling of the surface layer from 0 to 10 cm (0–1, 1–5, and 5–10 cm) was conducted to explore the effect of the diverse landscape on colloids in the modern layers. We hypothesized that (1) the WDC composition in the top layer (0–1 cm) among the different pits was mainly affected by the dry deposition and eolian reworking; (2) the depth distribution of WDCs was mainly related to leaching process induced by occasionally rainfall; and (3) colloidal P may work as a tracer for differences in nutrient distributions among sites with disturbance of other elements.

2. Methods and materials

2.1. Field sites and sampling

Sample sites were located along a topographic transect crossing the same alluvial fan system initially studied for n = 2 sites only by Moradi et al. in 2019 (Fig. 1a). The alluvial fan system is located in the hyper-arid region of Paposo (approximately 25°0′52″S, 70°20′8″W), which has a mean annual temperature of 17.2 °C and mean annual precipitation of <0.1 mm (Quade et al., 2007). The study transect is situated at 1480 m.a.s.l., positioned within the central portion of the alluvial fan (Fig. 1b). This location not only receives the input of materials from the upper sections but also undergoes the release of fine particles during rainfall events. The transect shows a variety of landscapes. Furthermore, one section within the transect has been marked by the presence of several shrubs (Fig. 1c, Fig. 3a). In order to increase replicates, a total of 11 sites were sampled based on the topographic characteristics along the transect of the alluvial fan system, including P1 on the hillslope, P2–P7 in the younger fan section, P8 on the edge/at the transition between the older and younger fan sections, and P9–P11 in the older fan section (Fig. 1b, Fig. 1c). Among the 7 sample sites located in the younger fan section, P2 and P3 belong to a modern channel, whereas P7 was dug in a channel that seemed to be inactive during recent flooding (Fig. 2). There are sparse, dry shrubs (*Huidobria fruticosa*) located in the younger fan section (Mörchen et al., 2021). P3 was sampled downward from one such shrub, P4 was collected in the direct vicinity of a shrub, and P6 was dug upward from a shrub.

Sampling was performed in March 2020. At each site, we collected soil samples from the land surface to a depth of 10 cm below the surface (b.s.), divided into three layers: 0–1 cm, 1–5 cm, and 5–10 cm. Sampling took place after removal of loose rocks and plant debris. Depth profiles were then sampled at regular intervals of 10 cm up to a depth of 50–80 cm b.s. (Fig. 2). The maximum sampled depth was set by practical constraints on digging e.g., presence large rocks or hardpans, which cannot be broken up and dug through without the use of pneumatic hammer. Spades and pickaxes were used to dig the pits in the younger fan section, and a demolition-type jackhammer was used to dig the pits in the older fan section as the ground was hard and consolidated. Drone flights were used to obtain a full picture of the geomorphological terrain

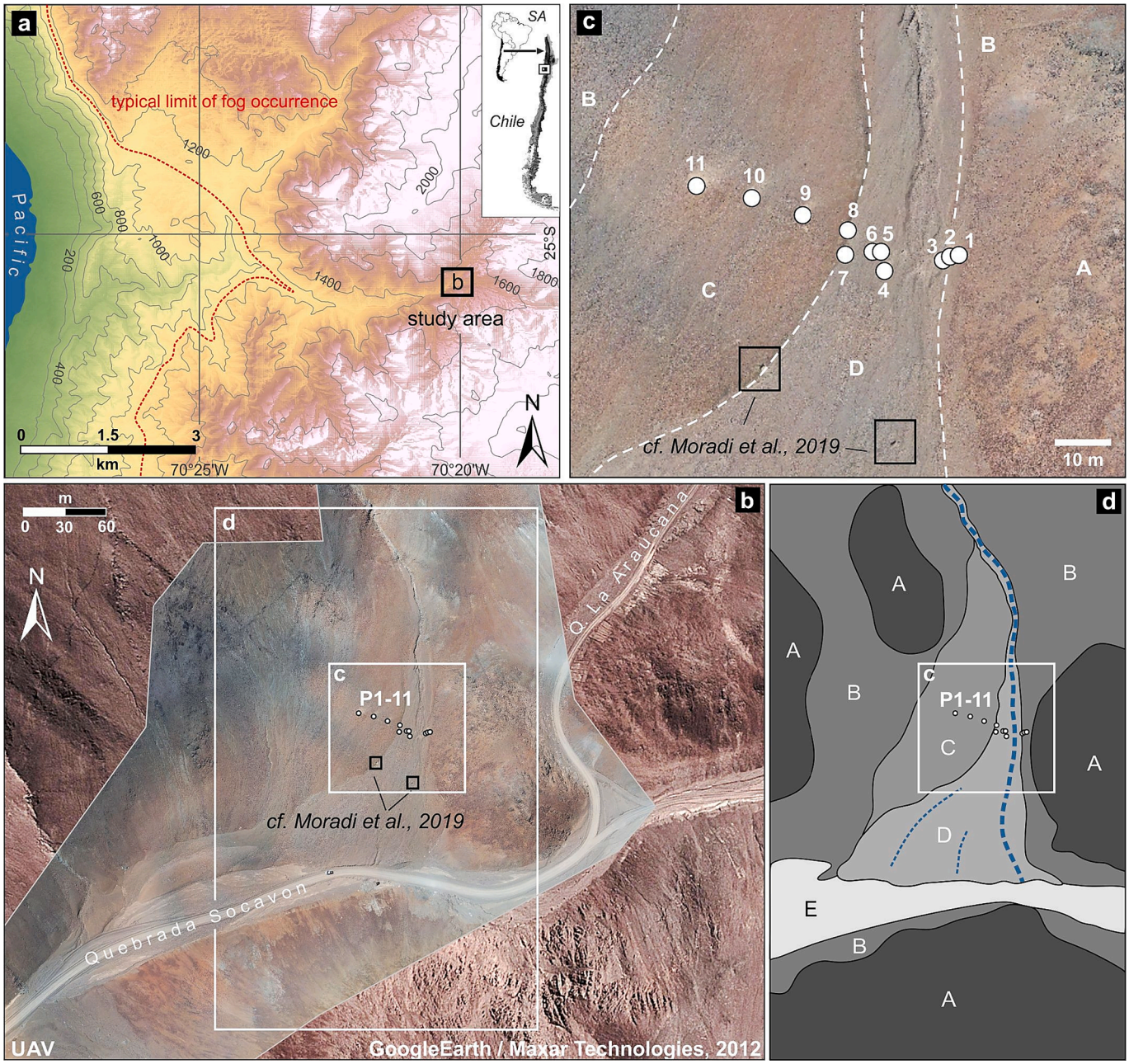

Fig. 1. Study area. (a) Digital elevation model of the study area at 1480 m.a.s.l.; the upper limit of the fog bank is typically around 1100 m. (b & c) Position of soil profiles on the fan, showing the two different alluvial fan sections, with red colors dominating the abandoned surface, and gray to brown colors indicating the younger and active fan section. (d) Geomorphology units of the study sites: A-Bedrock, B-Hillslope deposits/scree deposits, C-Older (inactive) alluvial fan generation, D-Younger (active) alluvial fan generation, E-Modern flood plain, Dotted blue line-Water pathway. P1–P7 belong to the younger fan section, P8 is at the transition between the older and younger fan sections, and P9–P11 are in the older fan section.

context for the alluvial fan system and sampling sites (Fig. 1b).

2.2. Optically stimulated luminescence (OSL) dating

Optically stimulated luminescence (OSL) dating analysis for the two sections (the older fan section and the younger fan section) was conducted at the Institute of Geography, University of Cologne. Pretreatment for burial dose determination followed standard procedures to extract potassium feldspars in the grain-size fraction 150–200 μm. Equivalent dose measurements were performed using a post-infrared infrared protocol with a stimulation temperature of 225 ℃ ($pIRIR_{225}$; Buylaert et al., 2009). The appropriateness of the protocol was confirmed by means of dose recovery tests (dose recovery ratios of 1.00 ± 0.01 and 1.03 ± 0.01) and residual dose measurements (<1% of the natural dose). Since equivalent dose distributions (with 12 aliquots each) do not indicate incomplete signal resetting prior to deposition, the central age model (Galbraith et al., 1999) was used for burial dose calculation. Dose rates were based on radionuclide concentrations of the sediment determined using high-resolution gamma spectrometry and the empirical potassium content of the feldspars of 10 ± 2% (Smedley et al., 2012). Dose rate and age calculations were performed using DRAC software (Durcan et al., 2015). Since fading measurements revealed g-values of <1.5%/decade, no fading correction was conducted.

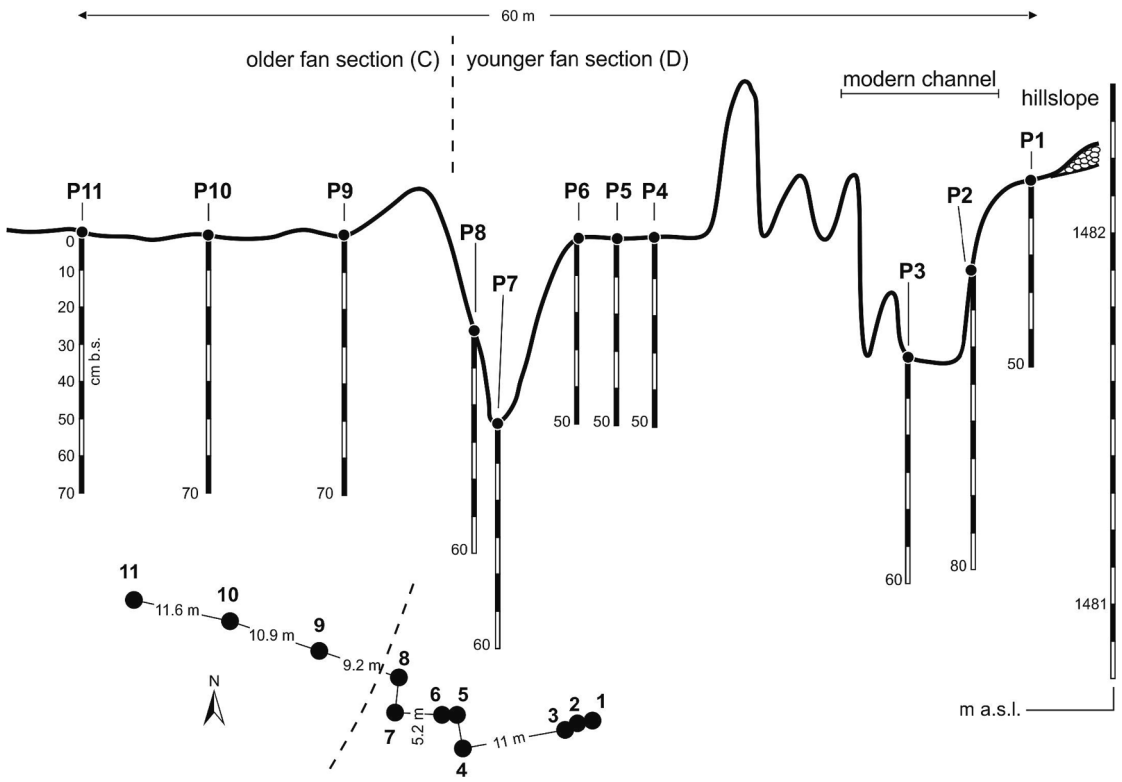

Fig. 2. Profile map of the soil samples from the alluvial fan system shown in Fig. 1(b & c); P1–P7 belong to the younger fan section, P1 is on the hillslope, P2–P3 are in a modern channel, P8 is at the transition between the older and younger fan sections, and P9–P11 are in the older fan section.

2.3. Water-dispersible colloid (WDC) extraction

Desert soils were air dried in situ before sampling and sieved to smaller than 2 mm without stones in order to perform water-dispersible colloid (WDC) analysis. WDC extraction was performed based on a commonly used procedure (Séquaris & Lewandowski, 2003). In brief, approximately 10 g of soil was mixed with 20 ml of Milli-Q water (1:2) and shaken on a horizontal shaker at 150 rpm for 6 h. An additional 60 ml of deionized water was then added to the suspension before sedimentation. To remove particles larger than 20 μm, a sedimentation time of 10 min was applied, which was calculated according to Stokes' law. The supernatant containing the non-settling phase was transferred by pipette to centrifugation tubes. The desired colloids <300 nm were obtained by centrifuging for 10 min at 7500 rpm. The centrifugation time was calculated based on Hathaway (2018). Furthermore, dynamic light scattering (DLS) (Nano ZetaSizer, Malvern) measurements were performed to determine the size range of the separated WDCs.

2.4. Asymmetric flow field-flow fractionation (AF4)

The WDCs <300 nm were freshly size separated by means of asymmetric flow field-flow fractionation (AF4) (AF2000, Postnova Analytics, Landsberg, Germany). AF4 coupled online with organic carbon detection (OCD; DOC-Labor, Karlsruhe, Germany) was used to determine the WDC-OC content, while colloidal Mg, Al, Si, P, Ca, and Fe were measured using online inductively coupled plasma mass spectrometry (ICP-MS; Agilent 7500, Agilent Technologies, US). The parameters of the AF4 separation method were determined based on the previously mentioned study by Moradi et al. (2020) and are shown in Table S1. To evaluate the particle size resolution of field-flow fractionation (FFF) separation, the same method was used to analyze latex standards as reference materials on the basis of samples (Moradi et al., 2020).

2.5. Statistical analysis

In this study, the formation age of alluvial fan and presence of plant were considered as two independent variables. The alluvial fan system was divided into three sections: the younger fan section far away from plants (P2, P5, and P7), the younger fan section near plants (P3, P4 and P6), and the older section with an absence of plants (P9, P10, P11). Levene's and Shapiro-Wilks tests were conducted to ensure that the data were normally distributed and had homogeneous variances. Then, independent-samples *t* tests ($P < 0.05$) for WDC-P content, the relative proportions of elements in WDCs, Si/Al and the fractions of WDCs were performed at a given depth to determine the significant differences by the soil age and presence of plant, respectively. Depth of 40–50 cm was the deepest comparison layer because P4 and P5 were sampled up to this depth. One-way ANOVA tests ($P < 0.05$) were conducted to determine the statistical differences of WDC-P content among soil profile (above 50 cm) in different fan sections. Pearson correlations were used to assess the relationships between P with the elements OC, Mg, Si, Al, Ca, and Fe in WDCs of three different size subfractions. Statistical analyses were conducted using SPSS v22.0 software (IBM, USA). All figures were constructed using the OriginPro v9.1 software (OriginLab, USA).

3. Results

3.1. Geomorphological characteristics and chronology information

The alluvial fan is 80 m wide and ~200 m long and has a typical triangle-shaped form (Fig. 1b). Together with its direct surrounding surfaces, the system contains 4 main geomorphological units including bedrock, hillslope deposits/scree deposits, an older (inactive) alluvial fan generation, and a younger (active) alluvial fan generation (Fig. 1d), with the latter indicating a multi-phase evolution of the fan. The older and the younger fan sections are separated by a ~0.8 m-high topographic step (Fig. 2, Fig. 3b).

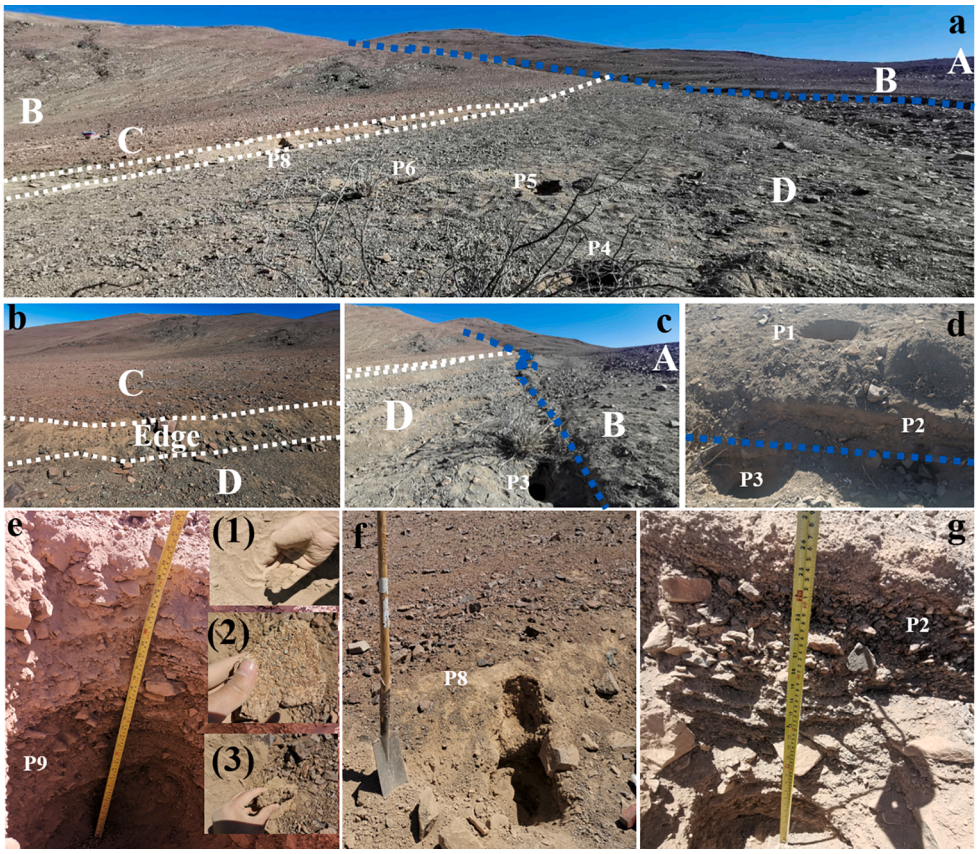

Fig. 3. Morphological characteristics of the alluvial fan. (a) Overview panorama photo of the alluvial fan at Paposo 1480 m.a.s.l.; A-Bedrock, B-Hillslope deposits/scree deposits, C-Older (inactive) alluvial fan generation, D-Younger (active) alluvial fan generation, Dotted blue line-Water pathway. (b) Surface of the older fan section and edge/transition between the older and younger fan sections. (c) Surface of the younger fan section. (d) Sample sites P1, P2, and P3. (e) Profile of the older fan section (P9), with (1) fine particles at the surface and (2 & 3) a ~3 cm mineral/salt solid layer at 5–10 cm. (f) Edge profile of P8. (g) Profile of the younger section (P2).

The surface of the younger fan section is characterized by distinct bar-and-swale topography with 0.1 to 0.5 m relief (Fig. 2). Sparse plants and clasts ranging from pebbles to cobbles were observed on the well-packed pavement surface (Fig. 3a & c). The alluvial sediments and soil layers exhibit gray colors and rather loose bedding (Fig. 3g). The profiles in this younger section have a distinct stratigraphy with well-defined layers of different grain size (Fig. 3g). In contrast, the landscape of the older (inactive) fan section lacks plants (Fig. 3a). A mature desert pavement is present on the surface, with heavily varnished and rubified clasts ranging in size from cobbles to small boulders (Fig. 3a & b). Compared with the younger fan section, the older fan section is flat and does not exhibit bar-and-swale morphology (Fig. 3a & b). This inactive section is characterized by reddish sediment colors, indurated sediment layers, and a solid layer nearly 3 cm thick at a depth of 5–10 cm below the surface (Fig. 3e). The P8 soil profile, which is located at the edge of the older fan section, showed similar indurated sediment characteristics, though without a solid layer in the 5 to 10 cm layer (Fig. 3f). OSL ages in the younger and active fan section (sample F2) date to ~13.6 ka, while sediments from the older and inactive fan section (F1) have an age of ~56.4 ka (Table 1).

3.2. Size fractionation and elemental distribution of WDCs in the surface layer (0–1 cm)

In the surface layer (0–1 cm), the concentrations of WDC—including both mineral elements and OC—amounted to around 65 ± 2.7 mg $kg^{-1}_{bulk\ soil}$ in samples from the younger fan section with an absence of plants (P2, P5, and P7) (Table S2). In comparison, the WDC content in samples from the older fan section (P9, P10, and P11) exhibited a larger range, from 54.8 mg kg^{-1} to 112.8 mg kg^{-1} soil (Table S2). The presence of shrubs increased the variation in WDC concentration from 61.2 mg kg^{-1} to 525.2 mg kg^{-1} in the surface layer from sites P3, P4, and P6 (Table S2). The elemental proportions of WDCs in the surface layer (0–1 cm) differed among three sections (Fig. 4, Table S3, Table S4, Fig. S2). In general, the contribution of Ca for WDCs was lower in the older than that of the younger one (Table S3). The OC accounted for the largest proportions of WDCs in samples collected near shrubs, increasing by one magnitude from 6.9 ± 3.4 to 68 ± 20% at younger fan section (Table S4).

Fractograms of the surface layer (0–1 cm) in all 11 soil profiles depicted three elemental peaks with similar elution time between samples (Fig. 4, Fig. 5). The first peak consisted of nanocolloids (NCs) with a size range of 0.6–24 nm (Moradi et al., 2020). The second peak from approximately 24 to 210 nm was related to fine colloids (FCs), and the third peak was associated with medium colloids (MCs) eluted from

Table 1
Optically stimulated luminescence (OSL) dating results of samples from the alluvial fan.

Sample[§]	U (ppm)	Th (ppm)	K (%)	DR (Gy/ka)	N	OD (%)	De (Gy)	g-value (%/dec)	Age unc. (ka)
F1	2.6 ± 0.2	13.3 ± 0.9	2.7 ± 0.1	5.2 ± 0.2	12	10 ± 3	261 ± 10	0.7 ± 0.1	56.4 ± 2.8
F2	2.7 ± 0.2	13.2 ± 0.9	2.5 ± 0.1	5.0 ± 0.2	12	44 ± 9	68 ± 9	1.5 ± 0.7	13.6 ± 1.8

[§] Both samples were taken at ~30 cm below the surface. U, uranium; Th, thorium; K, potassium; DR, dose rate; N, number of aliquots; OD, overdispersion; De, burial dose (in gray). The OSL dating was carried out in the Cologne Luminescence Laboratory.

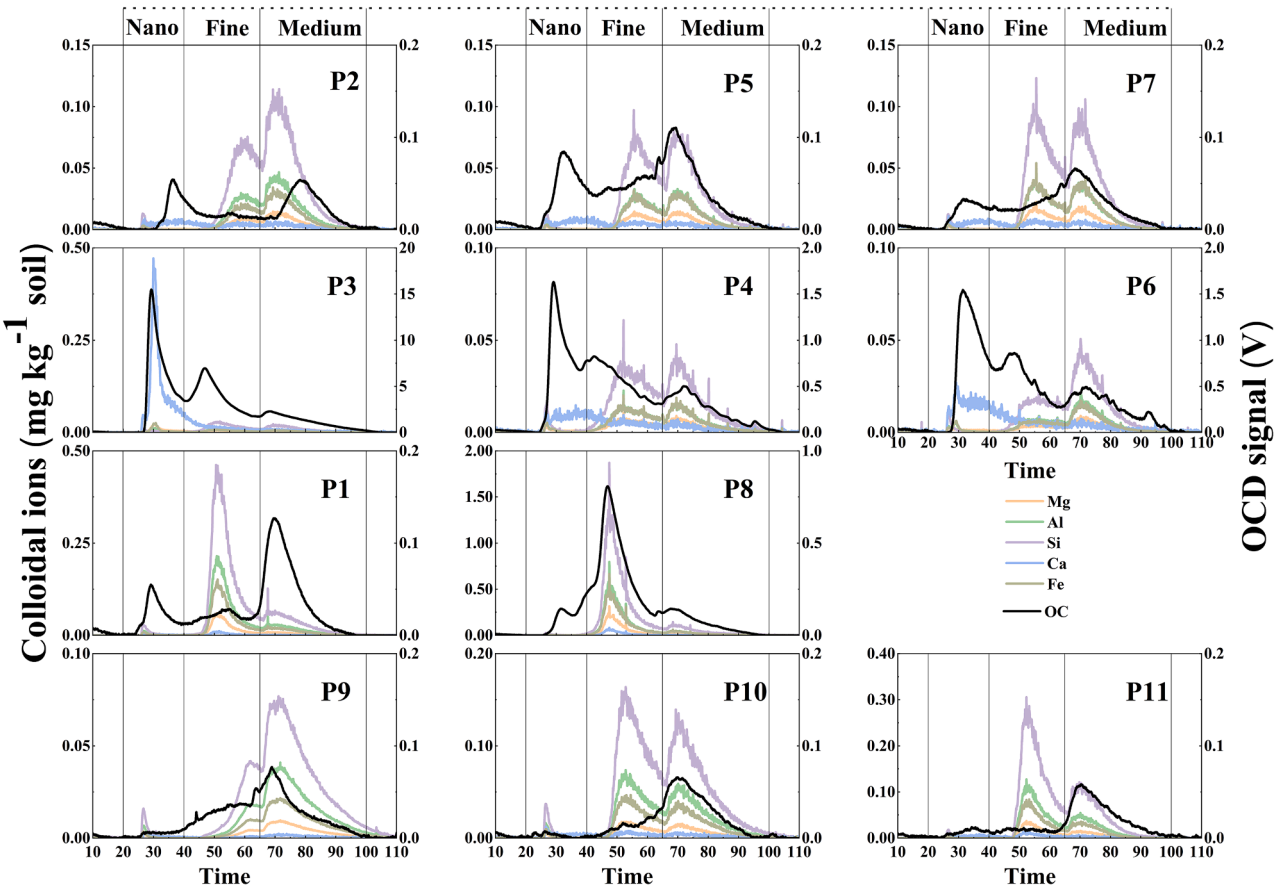

Fig. 4. Fractogram of water-dispersible colloid (WDC) elements, e.g., magnesium (Mg), aluminum (Al), silicon (Si), calcium (Ca), iron (Fe), and organic carbon (OC) in the top layer (0–1 cm) of soils at 11 sampling sites, obtained by flow field-flow fractionation (FFF) coupled with inductively coupled plasma mass spectrometry (ICP-MS) and organic carbon detection (OCD). P1 is on the hillslope, P2, P5 and P7 belong to the younger fan section with an absence of plants, P3, P4, and P6 are in the younger fan section near plants, P8 is at the transition between the older and younger fan sections, and P9–P11 are in the older fan section. Nano: Nanocolloid fraction from 0.6 nm to 24 nm; Fine: Fine colloid fraction from 24 nm to 210 nm; Medium: Medium colloid fraction from 210 nm to 300 nm. Note different scaling of Y-axes for the 11 figures.

210 to 300 nm. The three WDC sizes showed site-specific distribution patterns (Table S3, Table S4). The MCs were the dominant particle size of WDCs in the surface layer both of the younger fan section far away from plants (54 ± 7% of all WDCs) and the older fan section (54 ± 20% of all WDCs) (Fig. 4, Table S3). In contrast to the younger fan far away from plants, the NCs were significantly depleted at the surface soil samples from the older fan section (Table S3). Noteworthy, NCs were elevated while MCs decreased in samples collected near shrubs compared to those with an absence of plants (Fig. 4, Table S4). FCs, amounting to 39 ± 3% of all WDCs, were abundant in samples near plants (Fig. 4). Si, Al, and Fe showed similar fractogram trends and peaks and were the main constituent elements of fine- and medium-sized WDC fractions from the soil surface when no plants were present (Fig. 4, Fig. S4, Fig. S5). In contrast, the fractogram trends for OC and Ca were different from those for Al, Si, and Fe for all surface samples except those from P8 (Fig. 4). Most colloidal OC and Ca accumulated in the first (NC) and second peaks (FC) of the fractogram. Furthermore, the NCs were dominated by OC and Ca content for samples in the younger fan section (Fig. S3).

3.3. WDCs in soil horizons

Differences in the WDC content were apparent between samples in soil horizons (Fig. 6). There was no common pattern of WDC depth distribution among the samples taken from the younger fan section. The maximum amounts of colloids in the younger fan section were mainly detected below 10 cm (with the exception of P3 and P4) (Fig. 6, Table S2). Plant growth mainly affected soil properties of the top layer. WDCs in P3 and P4, the sites below or near the plant, reached a maximum of 525.2 and 112 mg kg^{-1} $_{bulk\ soil}$ at 0–1 cm (Table S2, Fig. 6, Table S4). The influence of fan age on overall distribution and composition of WDCs was not solely limited to the surface layer but extended to deeper in the profile (Table S4). Compared with sites in the younger fan section, the depth distributions of WDCs in the older fan samples were more homogeneous. The largest amount of WDCs was identified in the layer from 5 to 10 cm, with 163–561 mg kg^{-1} $_{bulk\ soil}$ in P9, P10, and P11 (Fig. 6, Table S2). For the most part, Si, Al, and Fe were identified as the predominant elements in each layer, and were abundant in both FC and MC fractions. The stoichiometric Si/Al ratio of WDCs at deeper layers (20–40 cm) was around 3 ± 0.2, which was significantly higher than that of samples from the younger fan section (2.5 ± 0.13). No more than 1 mg kg^{-1} $_{bulk\ soil}$ NC-OC was detected in profile from the older fan section, which was less than that found in most of the samples from the younger fan section, especially in sites near shrubs (Table S2). In P8, which is located on the topographic step between the younger and older fan generations, the maximum WDC content (367 mg kg^{-1} $_{bulk\ soil}$) was observed in the top layer (0–1 cm), with a sharply decreasing trend as depth increased (Fig. 6, Table S1).

3.4. Phosphorus (P) associated in the WDCs

No significant effect was induced by alluvial fan age on WDC-P

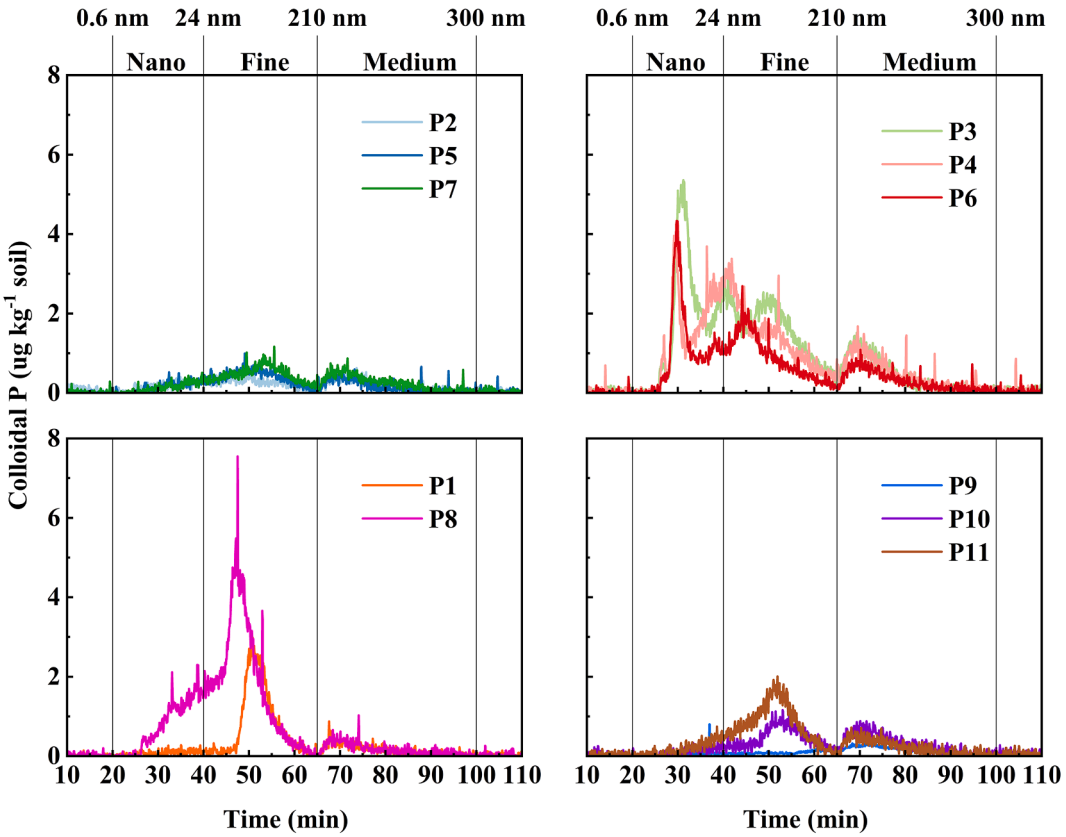

Fig. 5. Fractogram of nanocolloidal (Nano), fine-colloidal (Fine), and medium-colloidal (Medium) phosphorus (P) in the top layer (0–1 cm) of 11 samples analyzed by asymmetrical flow field-flow fractionation (AF4) coupled with inductively coupled plasma mass spectrometry (ICP-MS). P1 is on the hillslope, P2, P5 and P7 belong to the younger fan section with an absence of plants, P3, P4, and P6 are in the younger fan section near plants, P8 is at the transition between the older and younger fan sections, and P9–P11 are in the older fan section.

content in 0–1 cm while significantly more WDC-P (1.07 ± 0.3 mg kg^{-1} $_{bulk\ soil}$) were found in the samples collected near shrubs compared with sites with an absence of plants (0.28 ± 0.06 mg kg^{-1} $_{bulk\ soil}$) (Fig. 5, Fig. 7, Table S2). For the most sites, 42–68% WDC-P was associated with FCs while plants enhanced the contribution of NCs.

In general, the depth distribution of P content was comparable to the depth distribution of the WDC content, with some variations (Fig. 6, Fig. 7, Fig. S6). WDC-P increased substantially in the sites near plants compared with other samples from the younger fan section not located near shrubs (Fig. 7). Noteworthy, WDC-P had accumulated significantly at 5–10 cm in the older fan section (Fig. 7). WDC-P was predominantly carried by FCs in all profiles (Fig. 7). Correlation analysis results showed that the dominate FC-P was significantly correlated with both mineral elements (Si, Ca, Fe, and Al) and OC in all samples (Table S5). NC-P was identified to cluster with OC in samples located on the younger fan section while it was significantly correlated only with mineral elements in samples from the older fan section. MC-P in samples collected near shrubs (P3, P4 and P6) was strongly correlated with OC and Ca, while it was significantly correlated with mineral elements (Si, Ca, Fe, and Al) in samples collected under the absence of shrubs in the younger fan section (P2, P5, P7) and samples located on the older fan section (P9, P10, P11) (Table S5).

4. Discussion

4.1. The formation age of the alluvial fan and its surface characteristics

The Coastal Cordillera is a narrow mountain range with predominant elevations of ~1000–2000 m a.s.l. While numerous large coastal alluvial fans are found in elevations of <200 m a.s.l. along the western margin of the Coastal Cordillera between 20.5°S and 25.5°S (Bartz et al., 2020; Walk et al., 2020; Walk et al., 2023), medium-sized alluvial fans with gently sloping surfaces (~2–6°) are typically found at intermediate elevations of the Coastal Cordillera, where they feed the episodically active stream channels of the larger Quebradas. As located in the hyper-arid region with mean annual precipitation of <0.1 mm, alluvial fan and stream channel activation mainly occurs during El Niño-related precipitation events (Haug et al., 2010; Sager et al., 2021). The alluvial fan system studied here is characterized by slopes of approximately ~5–6° and is therefore typical for this part of the hyper-arid Coastal Cordillera. Furthermore, as characteristic for numerous alluvial fans in general but also in this part of the Coastal Cordillera, the studied alluvial fan shows inactive/abandoned and younger/active sections, with the active/younger areas incised into the older part of the fan (Riquelme et al., 2003; Walk et al., 2023).

The aridification process in the hyper-arid core of the Atacama Desert has been ongoing from at least ca. 9 Ma to 37 Ma, although it has been interrupted by several wetter periods or periods of less arid conditions (Dunai et al., 2005; Rech et al., 2006; Ritter et al., 2019). Alluvial fan formation and, thus, the deposition of the sediments investigated in this study occurred during the late Pleistocene, likely during periods with increased moisture availability and/or precipitation. The OSL data revealed that the older section of the alluvial fan was active around ~56 ka, whereas the sediments of the younger section dated back to ~14 ka, which is consistent with more humid periods recorded in the hyper-arid core of the Atacama Desert (Bartz et al., 2020; Diederich et al., 2020; Ritter et al., 2019). For instance, the intervals from 75.7 to 60.7 ka and from 53.4 to 15.3 ka were identified as humid phases based on the paleoclimate record of the Salar der Atacama (~23°S) (Bobst et al., 2001). Furthermore, in the area of 22–24°S, more humid conditions

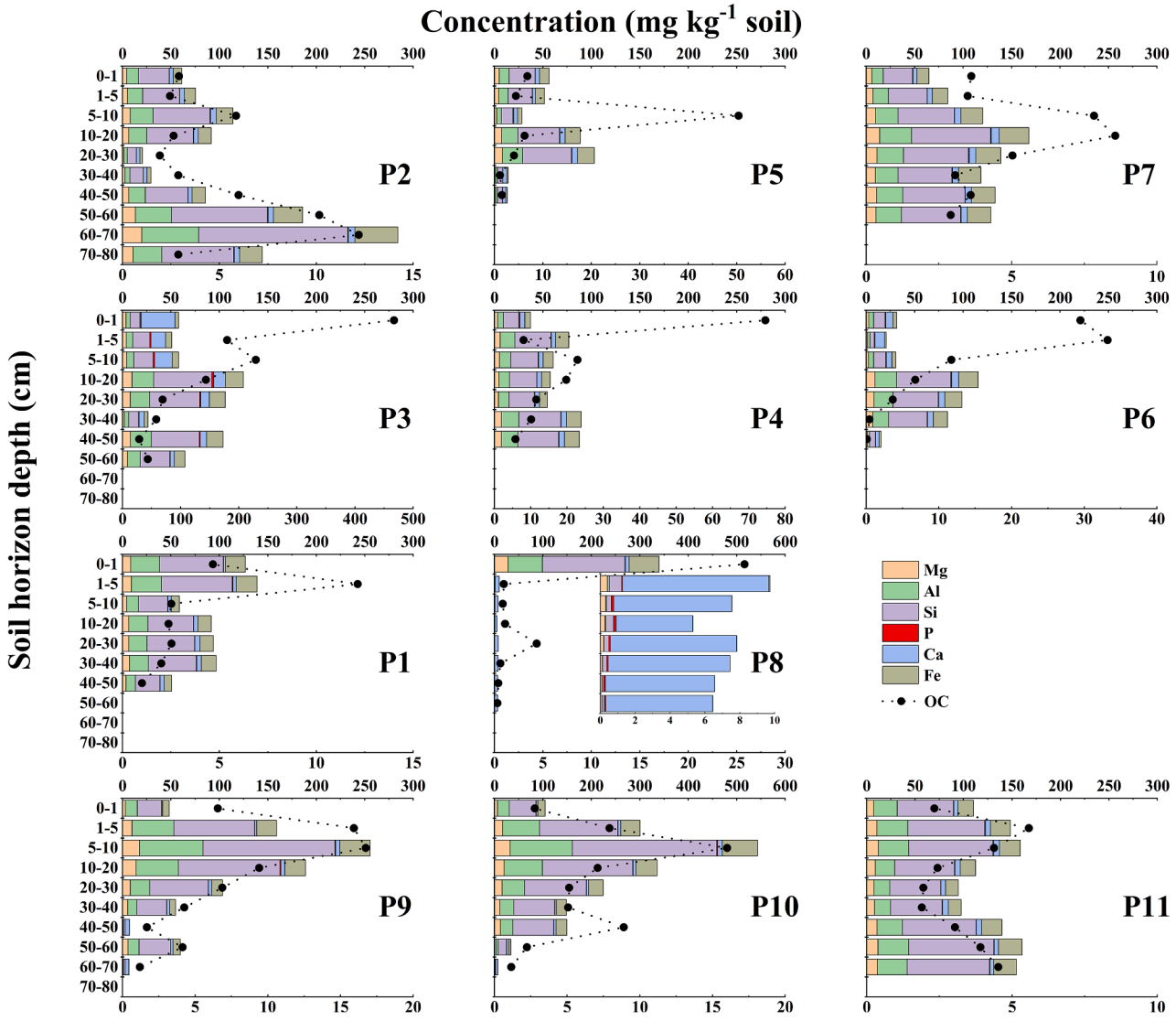

Fig. 6. Element concentrations of WDCs at different soil depths in the alluvial fan. P1 is on the hillslope, P2, P5 and P7 belong to the younger fan section with an absence of plants, P3, P4, and P6 are in the younger fan section near plants, P8 is at the transition between the older and younger fan sections, and P9–P11 are in the older fan section. Top horizontal axis and bars represent the concentrations of colloidal elements, e.g., magnesium (Mg), aluminum (Al), silicon (Si), phosphorus (P), calcium (Ca), and iron (Fe). Bottom horizontal axis and dotted line represent OC concentrations.

were also documented from 15 to 10 ka (Latorre et al., 2002). Although the reasons for the formation of the distinct topographical step between the older and younger fan generations remain unclear, the depositional activity in the alluvial fan seems to have ceased with the transition to dryer conditions at the beginning of the Holocene. Later, the alluvial fan surface was preserved during the more arid conditions prevailing throughout the Holocene, as previously observed in the Atacama (Amundson et al., 2012; Placzek et al., 2010). While the data thus suggests that soil formation-type processes started at ~56 ka on the older alluvial fan surface, and at ~14 ka on the younger alluvial fan surface, atmospheric inputs of soluble salts and insoluble particles that accumulated in the soil surface are prone to aeolian relocation with extremely slow erosion rates. Moreover, it can generally be assumed that leaching processes were absent during the dry period (Arenas-Díaz et al., 2022).

Compared with the older fan section, the younger fan section showed a higher surface roughness with more small-scale topographic variations (Fig. 2, Fig. 3). The surface of the alluvial fan tends to be smoother in the older section, where the bars and swales observed in the younger fan section are absent (Frankel & Dolan, 2007). In general, the continuing accumulation of sulphate-rich aeolian dust in the surface layer has resulted in the dramatic volumetric expansion and smoothed appearance of the landscape in the central Atacama (Clarke, 2006; Ewing et al., 2006; Rech et al., 2003). As a result, desert pavements weakly cemented by a thin sulphate crust with an overlying layer of more powdery dust are a common feature of the architecture in the Atacama Desert, and were also observed in the older fan section (Clarke, 2006). Therefore, 7 sample sites were selected within the younger fan section to effectively illustrate the impact of varied topographic characteristics on distribution of fine particles while 3 samples were chosen on the older fan section.

4.2. WDCs in the surface layer (0–1 cm) affected by topographic variations

The top layer from 0 to 1 cm belongs to the local regolith, which shows susceptibility to the input of fresh fine particles from atmospheric deposition and reworking due to weathering erosion (Sun et al., 2018; Li et al., 2019). Based on an estimated age of ~6.6 Ma, Wang et al. (2015) found a soil buildup of 2.25 m in the Atacama Desert via soil formation

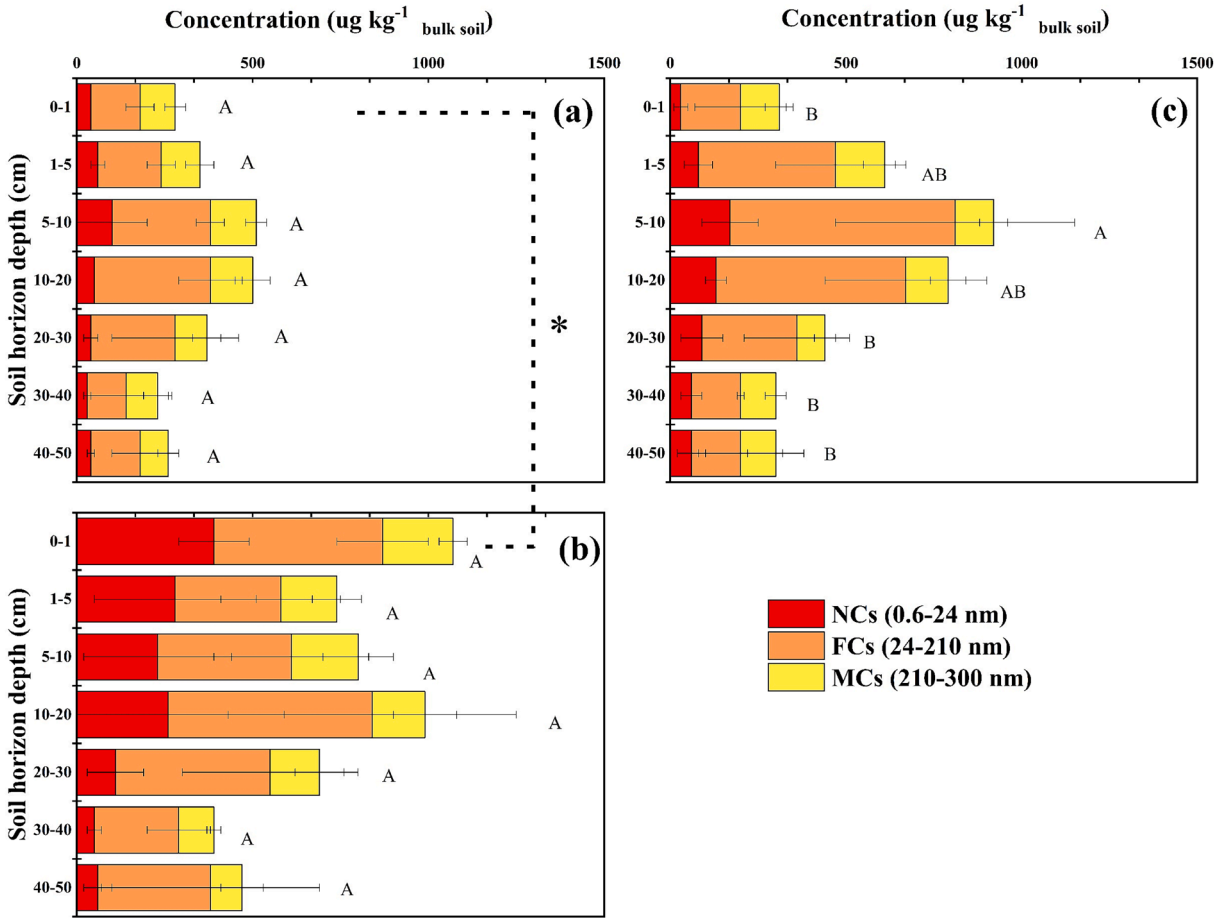

Fig. 7. P concentration in three different WDC subfractions (NCs-Nanocolloids, FCs-Fine colloids, MCs-Medium colloids) at three fan sections: (a) samples belong to the younger fan section far away from plants including P2, P5 and P7, (b) samples in the younger fan section near plants including P3, P4, and P6, and (c) samples in the older fan section with an absence of plants including P9, P10 and P11. Different uppercase letters indicate significant difference of WDC-P among soil profile for the younger fan section far away from plants, the younger fan section near plants and the older fan section with an absence of plants, respectively (one-way ANOVA with Tukey's HSD test; $P < 0.05$). Significant difference of plant growth (a, b) is shown with star.

and deposition; at this buildup rate, the surface soil (0–1 cm) may form over nearly 2.9 ka. The age of soil formation at 0–1 cm is younger than that the overall age of the younger fan section. Thus, the WDC fractograms from the 0–1 cm layer were analyzed to identify the topographic influences on the concentration, composition, and distribution of soil colloidal fractions (Fig. 4). A larger variation in WDC content and dominant size fractionations were identified in samples from the older fan section (P9, P10, and P11) than in samples from the younger fan section with an absence of plants (P2, P5, and P7) (Fig. 4, Table S2, Table S3). The heterogeneous characteristics of the surface WDCs in samples from the older fan section (P9, P10, and P11) may be due to spatially uneven soil formation processes such as dust deposition or aeolian reworking. The smooth top layer of the older fan section with its increased soil erodibility may activate dust emission and random transportation by winds (Hennen et al., 2022), thus leading to a spatially heterogeneous distribution of colloids. A greater surface roughness is beneficial for capturing atmospheric deposition particles (aerosols and dust) and can reduce soil erodibility by winds (Arenas-Díaz et al., 2022; Ewing et al., 2006; Finstad et al., 2016). As a result, the smaller surface disturbance of WDC concentration and distribution was related to a larger surface roughness in samples from the younger fan section with an absence of plants. Though the surface layer of P8 (at the transition between the older and younger fan sections) was detected as part of the reddish sediment at the edge of the older fan section, the WDC patterns from P8 were different from those of other soil samples from the older fan section (P9, P10, and P11). The results confirmed that topographic variations had a major impact on colloid distribution, and may support the higher randomness of aeolian reworking on the surface layer, which is more exposed to winds. The size distributions of WDCs does not only reflect particle release upon water contact, but may well also reflect changes in particle aggregation (Jiang et al., 2015b; Zhang et al., 2021). The main reason for the lacking peaks in NC signals for the samples from the older fan section (P9, P10, and P11) could thus indicate both, that they were blown-off as indicated above, or additionally aggregated to larger colloids with time. In either way, lower portions of NCs coincided not only with different topographic morphology but also with different fan ages (Table S3).

Calcium which was even not classified as the major element of WDCs for the surface diminished even further with time (Table S2, Table S3). In the Atacama Desert, the main source of calcium (Ca) is the accrual of salts such as $CaCO_3$ and $CaSO_4$, which originate from windblown dust from the Pacific Ocean and/or from aeolian reworking aerosols (Ewing et al., 2006; Clarke, 2006; Rech et al., 2003). $CaCO_3$ contents decreased with an increasing age of alluvial fan systems in Paposo area (Ewing et al., 2006; Walk et al., 2023). Higher WDC-Ca content was found in 1–5 cm layer of our older fan section, which may support the assumption that more Ca was translocated here through leaching processes over time (Fig. 6, Table S3). Indeed, larger amounts of Ca assemble in aridic soils is due to less loss by leaching processes (Wang et al., 2014; Li et al., 2019; Oerter et al., 2016). Note, upward migration due to evaporative processes induces the accumulation of Ca on the surface during long-term arid periods (Pfeiffer et al., 2021).

4.3. WDCs in the surface layer (0–1 cm) affected by plants

In our study, the WDC-OC and WDC-Ca content in the surface layer (0–1 cm) was higher in samples collected near shrubs (P3, P4, and P6) than in samples with an absence of plants (P2, P5, and P7) from the younger fan section (Fig. 4, Table S2). Higher WDC-OC concentration in soils may be caused by increased soil OC inputs due to plant growth (Yan et al., 2018; Zhang et al., 2021). The orientation of samples in relation to plants had a strong effect on the magnitude of WDC-OC concentration isolated from the bulk soil (Fig. 4). WDC-OC in P3, which is located downward from a plant, was 467 mg kg^{-1} $_{bulk\ soil}$, which was higher than that in both P4 (74.5 mg kg^{-1} $_{bulk\ soil}$)—located in the direct vicinity of a plant—and P6 (29.5 mg kg^{-1} $_{bulk\ soil}$), which is located upward from a plant (Table S2). The varied distribution of plant litters in the surface layer may be mainly due to the occasional rainfall. The downslope waterflow may lead to the accumulation of more plant litters in sites downward from plants, such as P3 (Fig. 3c). In addition, winds may also play an important role in material scavenging and transportation in desert systems (Jacques-Coper et al., 2015; Reyers et al., 2019). The sites downward from the shrubs located in the modern channel provide a shelter from transportation by wind, which may increase material accumulation.

Net Ca mineralization from decomposing plant debris can increase the Ca amounts in bulk soil (Dijkstra, 2003). This may be one of the reasons for the higher WDC-Ca identified in the surface layer from samples collected near shrubs (P3, P4, and P6). However, with the exception of WDC-Ca, other WDC-bound mineral elements (Si, Al, Fe, and Mg) in the surface layer of samples sampled near shrubs decreased compared with those with an absence of plants (Fig. 4, Table S2, Table S4). This may be due to the formation of larger-sized soil aggregates between organic matter and inorganic compounds of the above elements under higher Ca ion concentrations in sites near plants (Totsche et al., 2018; Wang et al., 2020; Zhang et al., 2021).

With the higher WDC-OC and WDC-Ca amounts, NCs accounted for the largest proportion of WDC size fraction in the P3, P4, and P6 sites (Fig. 4, Table S4). The Ca^{2+} bridging effect with organic matter most likely contributed to NC formation, which was consistent with the results obtained by Li et al. (2021) for agricultural soils and by Wang et al. (2020) for calcareous forest soils.

4.4. Depth distribution of WDCs in younger and older alluvial fan sections

Various depth distributions of WDCs from the different sampling sites were determined for different sections of the alluvial fan system studied here (Fig. 6, Table S3, Fig. S1, Fig. S2). The maximum amounts of colloids were found in the soil layer from 5 to 10 cm in the older fan section (P9, P10, and P11). In contrast, the largest proportion of WDCs was accumulated below 10 cm in sites located in the younger fan section with no plants (Fig. 6, Table S2). The depth pattern of the younger fan section was synchronous with the results for the "Fan" section observed by Moradi et al. (2020), which showed the maximum WDC (<500 nm) concentrations at a depth of 10–20 cm. These results were considered to be mainly due to the absence of a hard layer in the surface (0–10 cm) of the "Fan" section with a higher infiltration rate (Moradi et al., 2020). The coarser soil texture detected in the "Fan" section facilitated in-situ translocation of colloidal particles (Table S6; Moradi et al., 2020). The total WDC concentration at the old fan site was not systematically lower than that in the young one, suggesting that aggregation processes with depth likely affected WDCs to a minor degree. The spatial variability of WDC depth distribution in our study can, therefore, at least be partly attributed to the different hydrological characteristics of the two sections. The average infiltration rate value of the active alluvial fan section seems to be higher compared with the inactive section, which displays similar surface features to the nearby hillslope. In a field study conducted between 22 and 26°S, Pfeiffer et al. (2021) estimated that the infiltration rate capacity of the alluvial fan was around 244 mm h^{-1}, while the value was 78 mm h^{-1} on the nearby hillslope. Physical, chemical, and biogenic crusts as well as stone cover are of great relevance for the hydrological response of desert soils to rainfall (Assouline, 2004; Belnap, 2006; Lavee & Poesen, 1991). In our study, a relatively more mature desert pavement is present on the older fan section surface, with heavily vanished and rubified clasts ranging in size from cobbles to small boulders (Fig. 3). This well-packed pavement may exhibit less permeability in the surface layer (Owen et al., 2013). Furthermore, the younger fan section may be conductive to infiltration because of its rough surface (Ma et al., 2022). Additionally, a solid mineral layer of nearly 3 cm thickness was observed in the 5–10 cm layer of the older fan section (Fig. 3e). The mobilization of colloidal particles caused by water flow during infiltration processes may be inhibited by this solid mineral layer at 5–10 cm, leading to the accumulation of WDCs (Fig. 6, Table S2). In addition to the contribution made by downward soil water movement, the upward migration of waters driven by evaporation resulted in the gathering of fine particles in a certain layer, which may also partially contribute to the formation of the solid layer (Amundson et al., 2008; Davis et al., 2010; Finstad et al., 2014).

An irregular depth distribution of WDCs was detected in the deeper layer below 10 cm in the older fan section, which was similar to the disordered depth distribution of sites from the younger fan section (Fig. 6). Due to the formation of composite modern and relict soil layers through the interplay between occasional fluvial events and persistent aeolian erosion (Williams et al., 2021), it was not possible to identify a common trend for WDC depth distribution. Thus, soil layers may reflect a multiphase history of pedogenesis. Evenstar et al. (2009) reported that regionally extensive planation surfaces were unlikely to have any chronostratigraphic significance due to their multiphase history. In addition, soil formation processes such as wind erosion or leaching may be spatially variable and provide discontinuous cover over the soil surface. Alcayaga et al. (2022) suggested that small playa records were not helpful in reconstructing the regional climatic history of the recent past because of the high spatial patchiness of the rainfall events that occurred.

The site from the "Crust" section sampled by Moradi et al. (2020) was located in the downhill direction of the P8 site in our study, at the transition between the older and younger fan sections, rather than in the older fan section (Fig. 1b). Coincident with the apportionment of WDCs in the "Crust" section, we observed a sharply decreasing trend in WDCs in P8 with decreasing depth (Fig. 6). All maximum element content was detected in the surface layer. WDCs (Si, Al, Fe, Ca, OC, and P) in the surface layer of the "Crust" section, i.e., from 0 to 10 cm, amounted to nearly 922 mg kg^{-1} $_{bulk\ soil}$ (Moradi et al., 2020). However, the surface layer in P8 referred to the layer from 0 to 1 cm. When the relevant content in P8 from 0 to 10 cm was calculated, a relatively lower concentration (386 mg kg^{-1} $_{bulk\ soil}$) was observed (Fig. 6, Table S2). WDC content below 10 cm in P8 was also lower than that in the "Crust" section analyzed by Moradi et al. (2020). The discrepancy may be due to the different size of the WDCs extracted: we extracted colloids <300 nm, while they extracted <500 nm WDCs. In addition, the downslope movement of fine particles through lateral flow in surface and subsurface layers may enhance the discrepancy (Pfeiffer et al., 2021; Placzek et al., 2010). The accumulation of colloidal particles decreased in the direction of the hilltop and increased in the direction of the footslope.

Si and Al were present as the dominant elements in the colloids and the Si/Al ratio of WDCs in all samples collected without plants both from the younger and the older fan section, was more than 2 (Fig. 4, Table S2, Table S3). This result is in accordance with the findings obtained by Moradi et al. (2020), which identified that colloids not only originated from clay minerals (chlorite) but also from sand-derived particles. Multiple sources of the soils are involved in the Atacama Desert, including the erosion of silicate parent materials and the input of dust containing clay minerals, e.g., smectite, chlorite, and kaolinite (Amundson et al., 2012; Ewing et al., 2006; Moradi et al., 2020). It should be noted that the major atmospheric bulk deposition in inland

sites of the Atacama Desert was mineral assemblage (anorthite-gypsum-quartz-albite) (Wang et al., 2014). In the deeper 20–40 cm soil layer, the stoichiometric Si/Al ratio was significantly increased in the older fan compared to younger fan section without plants (Table S3). This may be due to more colloids released from silicate parent materials erosion with time in deeper layers.

4.5. P association to WDCs

Though colloidal P was detected in minor amounts in hyper-arid desert soils with 0.03–1.95 mg kg^{-1} bulk soil, P was enriched 11-fold in the WDCs in comparison to the bulk soil (P in bulk soil data referenced from Moradi et al., 2020) (Table S2, Table S6). In general, nutrients within WDC fractions are enriched compared with the bulk soil because of the high specific surface area (Missong et al., 2018a; Wang et al., 2020). When the fractogram for WDCs was compared with that for WDC-P, it was observed that the abundance of WDC-P was dependent on WDC elements (mineral elements and OC) in soils (Fig. 4, Fig. 5). However, the results of correlational analysis varied in different colloidal size fractions among different sampling sites, which provided more association details of P with colloids (Table S5). Phosphorus, usually exists as phosphate anion, likely associates with organic matter through cation bridging by bivalent cations (e.g., Ca^{2+}, Mg^{2+}) or binds to the positively charged mineral surface of amorphous Al and Fe oxides via electrostatic interaction (Li et al, 2020; Said-Pullicino et al., 2021; Regelink et al., 2015). OC was not involved in NCs in the associations of P with clay minerals from samples in the older fan section, which may be due to the negligible NC-OC in the smooth old section which was susceptible to wind erosion (Table S2, Fig. S3). The results showed that NC-P may be clustered with mineral elements (Ca, Mg, Fe, Al, Si) reasonably via charge interactions in the older fan section. In fact, OC was identified as a key component in the binding of P in FCs (Table S5). Fine-colloidal P (FC-P) fractions, which show the highest intensity of the three colloidal sizes in most soils (42–74%), were correlated with both mineral elements and OC in FCs no matter in the younger fan section or the older one (Table S5). As was determined for arable land by Li et al. (2021), FC-P was correlated with clay minerals and likely to form a complex of OC-clay-P. Clay minerals may presumably immobilize the P in the soil through adsorption, ligand exchange and precipitation (Amadou et al., 2022; Celi et al., 2001; Gérard, 2016). Jiang et al. (2015b) also identified that inorganic and organic P compounds sorbed strongly to the positively charged surfaces of the edge of clay minerals and that of amorphous Al and Fe (hydr)oxides. MC-associated P was correlated with OC and Ca in samples collected near plants, however, samples far from plants implied a fixation of P with Fe/Al (hydr)oxides or clay minerals in MCs (Table S5). Ca was present in large amounts along with a high concentration of OC in WDCs from samples near shrubs (P3, P4, and P6) (Table S2), which may form OC-Ca-P bridges (Jiang et al., 2023; Yang et al., 2019). Thus, more colloidal P was observed in the top layer (0–1 cm) of P3, P4 and P6, which contained large amounts of WDC-OC and WDC-Ca (Fig. 6, Fig. 7, Table S4).

5. Conclusion

The composition and distribution of water-dispersible colloids (WDCs, <300 nm) in the surface layer (0–1 cm) of the sample sites under hyper-arid conditions were affected by topographic variations, the age of natural soil development and vegetation cover. More nanocolloids (NCs, 0.6–24 nm) and WDC-P were detected in the surface soil of samples collected near shrubs with more input of OC and Ca. An irregular depth distribution of WDCs was observed in the profile of samples from the younger fan section while WDCs accumulated in layers above 10 cm in samples from the older fan section. On the one hand, this can reflect the complex pedogenesis history of the deeper soil layers. However, on the other hand it likely indicates differences in the downward water flow, which was inhibited by a mineral/salt solid layer at the older fan sites, resulting in WDC accumulation at 5–10 cm. Hence, even in this hyper-arid environment, rare events of rain affected soil depth properties and therewith the overall (geo)ecology of the whole fan landscape.

Declaration of Competing Interest

The authors declare that they have no known competing financial interests or personal relationships that could have appeared to influence the work reported in this paper.

Data availability

Data will be made available on request.

Acknowledgements

This work was done as part of a Collaborative Research Center project: “Earth-Evolution at the Dry Limit,” funded by the Deutsche Forschungsgemeinschaft (DFG, German Research Foundation)–Projektnummer 268236062–SFB 1211. Additional funding support was provided by the Chilean ANID-MEC80190012. Xiaolei Sun thanks the China Scholarship Council (CSC:201904910544) for supporting her study at RWTH Aachen University and Forschungszentrum Jülich. The authors would like to thank Dr. Volker Nischwitz (ZEA-3, Forschungszentrum Jülich) for support with the FFF-ICP-MS measurements.

Appendix A. Supplementary data

Supplementary data to this article can be found online at https://doi.org/10.1016/j.geoderma.2023.116650.

References

Aguilar, G., Cabré, A., Fredes, V., Villela, B., 2020. Erosion after an extreme storm event in an arid fluvial system of the southern Atacama Desert: an assessment of the magnitude, return time, and conditioning factors of erosion and debris flow generation. Nat. Hazards Earth Syst. Sci. 20, 1247–1265.

Alcayaga, H., Soto-Alvarez, M., Laronne, J.B., Caamaño, D., Mao, L., Urrutia, R., 2022. Runoff volume and sediment yield from an endorheic watershed generated by rare rainfall events in the Atacama Desert. Geomorphology 400, 108107.

Amadou, I., Faucon, M.-P., Houben, D., 2022. New insights into sorption and desorption of organic phosphorus on goethite, gibbsite, kaolinite and montmorillonite. Appl. Geochem. 143, 105378.

Amundson, R., Ewing, S., Dietrich, W., Sutter, B., Owen, J., Chadwick, O., Nishiizumi, K., Walvoord, M., McKay, C., 2008. On the in situ aqueous alteration of soils on Mars. Geochim. Cosmochim. Ac. 72 (15), 3845–3864.

Amundson, R., Dietrich, W., Bellugi, D., Ewing, S., Nishiizumi, K., Chong, G., Owen, J., Finkel, R., Heimsath, A., Stewart, B., Caffee, M., 2012. Geomorphologic evidence for the late Pliocene onset of hyperaridity in the Atacama Desert. Geol. Soc. Am. Bull. 124 (7-8), 1048–1070.

Arenas-Díaz, F., Fuentes, B., Reyers, M., Fiedler, S., Böhm, C., Campos, E., Shao, Y., Bol, R., 2022. Dust and aerosols in the Atacama Desert. Earth Sci. Rev. 226, 103925.

Assouline, S., 2004. Rainfall-induced soil surface sealing: a critical review of observations, conceptual models, and solutions. Vadose Zone J. 3 (2), 570–591.

Bartz, M., Walk, J., Binnie, S.A., Brill, D., Stauch, G., Lehmkuhl, F., Hoffmeister, D., Brückner, H., 2020. Late Pleistocene alluvial fan evolution along the coastal Atacama Desert (N Chile). Global Planet. Change 190, 103091.

Belnap, J., 2006. The potential roles of biological soil crusts in dryland hydrologic cycles. Hydrol. Process. 20 (15), 3159–3178.

Bobst, A.L., Lowenstein, T.K., Jordan, T.E., Godfrey, L.V., Ku, T.-L., Luo, S., 2001. A 106 ka paleoclimate record from drill core of the Salar de Atacama, northern Chile. Palaeogeogr. Palaeoclimatol. Palaeoecol. 173 (1-2), 21–42.

Bol, R., Gruau, G., Mellander, P.-E., Dupas, R., Bechmann, M., Skarbøvik, E., Bieroza, M., Djodjic, F., Glendell, M., Jordan, P., Van der Grift, B., Rode, M., Smolders, E., Verbeeck, M., Gu, S., Klumpp, E., Pohle, I., Fresne, M., Gascuel-Odoux, C., 2018. Challenges of reducing phosphorus based water eutrophication in the agricultural landscapes of Northwest Europe. Front. Mar. Sci. 5, 276.

Buylaert, J.P., Murray, A.S., Thomsen, K.J., Jain, M., 2009. Testing the potential of an elevated temperature IRSL signal from K-feldspar. Radiat. Meas. 44 (5–6), 560–565.

Carretier, S., Tolorza, V., Regard, V., Aguilar, G., Bermúdez, M.A., Martinod, J., Guyot, J.-L., Hérail, G., Riquelme, R., 2018. Review of erosion dynamics along the major N-S climatic gradient in Chile and perspectives. Geomorphology 300, 45–68.

Celi, L., Presta, M., Ajmore-Marsan, F., Barberis, E., 2001. Effects of pH and electrolytes on inositol hexaphosphate interaction with goethite. Soil Sci. Soc. Am. J. 65 (3), 753–760.

Choobari, O.A., Zawar-Reza, P., Sturman, A., 2014. The global distribution of mineral dust and its impacts on the climate system: a review. Atmos. Res. 138, 152–165.
Clarke, J.D.A., 2006. Antiquity of aridity in the Chilean Atacama Desert. Geomorphology 73 (1-2), 101–114.
Davis, W.L., de Pater, I., McKay, C.P., 2010. Rain infiltration and crust formation in the extreme arid zone of the Atacama Desert, Chile. Planet. Space Sci. 58 (4), 616–622.
Davis, M., Matmon, A., Placzek, C.J., Mclntosh, W., Rood, D.H., Quade, J., 2014. Cosmogenic nuclides in buried sediments from the hyperarid Atacama Desert. Chile. Quat. Geochronol. 19, 117–126.
Diederich, J.L., Wennrich, V., Bao, R., Büttner, C., Bolten, A., Brill, D., Buske, S., Campos, E., Fernández-Galego, E., Gödickmeier, P., Ninnemann, L., Reyers, M., Ritter, B., Ritterbach, L., Rolf, C., Scheidt, S., Dunai, T.J., Melles, M., 2020. A 68 ka precipitation record from the hyperarid core of the Atacama Desert in northern Chile. Global Planet. Change 184, 103054.
Dijkstra, F.A., 2003. Calcium mineralization in the forest floor and surface soil beneath different tree species in the northeastern US. Forest Ecol. Manag. 175 (13), 185–194.
Dunai, T.J., González López, G.A., Juez-Larré, J., 2005. Oligocene-Miocene age of aridity in the Atacama Desert revealed by exposure dating of erosion-sensitive landforms. Geology 33 (4), 321.
Durcan, J.A., King, G.E., Duller, G.A., 2015. DRAC: dose rate and age calculator for trapped charge dating. Quat. Geochronol. 28, 54–61.
Evenstar, L.A., Hartley, A.J., Stuart, F.M., Mather, A.E., Rice, C.M., Chong, G., 2009. Multiphase development of the Atacama Planation Surface recorded by cosmogenic 3He exposure ages: Implications for uplift and Cenozoic climate change in western South America. Geology 37 (1), 27–30.
Ewing, S.A., Sutter, B., Owen, J., Nishiizumi, K., Sharp, W., Cliff, S.S., Perry, K., Dietrich, W., McKay, C.P., Amundson, R., 2006. A threshold in soil formation at Earth's arid-hyperarid transition. Geochim. Cosmochim. Ac. 70 (21), 5293–5322.
Finstad, K., Pfeiffer, M., Amundson, R., 2014. Hyperarid soils and the soil taxonomy. Soil Sci. Soc. Am. J. 78 (6), 1845–1851.
Finstad, K., Pfeiffer, M., McNicol, G., Barnes, J., Demergasso, C., Chong, G., Amundson, R., 2016. Rates and geochemical processes of soil and salt crust formation in Salars of the Atacama Desert, Chile. Geoderma 284, 57–72.
Frankel, K.L., Dolan, J.F., 2007. Characterizing arid region alluvial fan surface roughness with airborne laser swath mapping digital topographic data. J. Geophys. Res-Earth 112, F02025.
Galbraith, R.F., Roberts, R.G., Laslett, G.M., Yoshida, H., Olley, J.M., 1999. Optical dating of single 698 and multiple grains of quartz from Jinmium rock shelter, Northern Australia: part 1, experiment design 699 and statistical models. Archaeomertry 41, 339–364.
Gérard, F., 2016. Clay minerals, iron/aluminum oxides, and their contribution to phosphate sorption in soils — A myth revisited. Geoderma 262, 213–226.
Ginoux, P., Prospero, J.M., Gill, T.E., Hsu, N.C., Zhao, M., 2012. Global-scale attribution of anthropogenic and natural dust sources and their emission rates based on MODIS Deep Blue aerosol products. Rev. Geophy. 50, 1–36.
Hathaway, J.C., 2018. Procedure for clay mineral analyses used in the sedimentary petrology laboratory of the U.S. Geological Survey. Clay Miner. 3 (15), 8–13.
Haug, E.W., Kraal, E.R., Sewall, J.O., Van Dijk, M., Diaz, G.C., 2010. Climatic and geomorphic interactions on alluvial fans in the Atacama Desert, Chile. Geomorphology 121 (3-4), 184–196.
Hennen, M., Chappell, A., Edwards, B.L., Faist, A.M., Kandakji, T., Baddock, M.C., Wheeler, B., Tyree, G., Treminio, R., Webb, N.P., 2022. A North American dust emission climatology (2001–2020) calibrated to dust point sources from satellite observations. Aeolian Res. 54, 100766.
Houston, J., 2006. The great Atacama flood of 2001 and its implications for Andean hydrology. Hydrol. Process. 20 (3), 591–610.
Jacques-Coper, M., Falvey, M., Muñoz, R.C., 2015. Inter-daily variability of a strong thermally-driven wind system over the Atacama Desert of South America: synoptic forcing and short-term predictability using the GFS global model. Theor. Appl. Climatol. 121 (1-2), 211–223.
Jiang, X., Bol, R., Nischwitz, V., Siebers, N., Willbold, S., Vereecken, H., Amelung, W., Klumpp, E., 2015a. Phosphorus containing water dispersible nanoparticles in arable soil. J. Environ. Qual. 44 (6), 1772–1781.
Jiang, X., Bol, R., Willbold, S., Vereecken, H., Klumpp, E., 2015b. Speciation and distribution of P associated with Fe and Al oxides in aggregate-sized fraction of an arable soil. Biogeosciences 12 (21), 6443–6452.
Jiang, X., Wulf, A., Bol, R., Klumpp, E., 2023. Phosphorus content in water extractable soil colloids over a 2000 years chronosequence of paddy-rice management in the Yangtze River Delta, China. Geoderma 430, 116296.
Jordan, T.E., Lohman, R.B., Tapia, L., Pfeiffer, M., Scott, C.P., Amundson, R., Godfrey, L., Riquelme, R., 2020. Surface materials and landforms as controls on InSAR permanent and transient responses to precipitation events in a hyperarid desert, Chile. Remote Sens. Environ. 237, 111544.
Jungers, M.C., Heimsath, A.M., Amundson, R., Balco, G., Shuster, D., Chong, G., 2013. Active erosion-deposition cycles in the hyperarid Atacama Desert of Northern Chile. Earth Planet. Sc. Lett. 371–372, 125–133.
Latorre, C., Betancourt, J.L., Rylander, K.A., Quade, J., 2002. Vegetation invasions into absolute desert: a 45, 000 yr rodent midden record from the Calama-Salar de Atacama basins, northern Chile (lat 22°-24°S). Geol. Soc. Am. Bull. 114 (3), 349–366.
Latorre, C., Betancourt, J.L., Rylander, K.A., Quade, J., Matthei, O., 2003. A vegetation history from the arid prepuna of northern Chile (22–23°S) over the last 13 500 years. Palaeogeogr. Palaeoclimatol. Palaeoecol. 194 (1–3), 223–246.
Lavee, H., Poesen, J.W.A., 1991. Overland flow generation and continuity on stone-covered soil surfaces. Hydrol. Process. 5 (4), 345–360.
Li, F., Liang, X., Li, H., Jin, Y., Jin, J., He, M., Klumpp, E., Bol, R., 2020. Enhanced soil aggregate stability limits colloidal phosphorus loss potentials in agricultural systems. Environ. Sci. Eur. 32, 17.
Li, J., Wang, F., Michalski, G., Wilkins, B., 2019. Atmospheric deposition across the Atacama Desert, Chile: Compositions, source distributions, and interannual comparisons. Chem. Geol. 525, 435–446.
Li, F., Zhang, Q., Klumpp, E., Bol, R., Nischwitz, V., Ge, Z., Liang, X., 2021. Organic carbon linkage with soil colloidal phosphorus at regional and field scales: insights from size fractionation of fine particles. Environ. Sci. Tech. 55 (9), 5815–5825.
Ma, Y., Li, Z., Deng, C., Yang, J., Tang, C., Duan, J., Zhang, Z., Liu, Y., 2022. Effects of tillage-induced soil surface roughness on the generation of surface-subsurface flow and soil loss in the red soil sloping farmland of southern China. Catena 213, 106230.
Missong, A., Bol, R., Nischwitz, V., Krüger, J., Lang, F., Siemens, J., Klumpp, E., 2018a. Phosphorus in water dispersible-colloids of forest soil profiles. Plant Soil 427 (1-2), 71–86.
Missong, A., Holzmann, S., Bol, R., Nischwitz, V., Puhlmann, H., v. Wilpert, K., Siemens, J., Klumpp, E., 2018b. Leaching of natural colloids from forest topsoils and their relevance for phosphorus mobility. Sci. Total Environ. 634, 305–315.
Moradi, G., Bol, R., Trbojevic, L., Missong, A., Mörchen, R., Fuentes, B., May, S.M., Lehndorff, E., Klumpp, E., 2020. Contrasting depth distribution of colloid-associated phosphorus in the active and abandoned sections of an alluvial fan in a hyper-arid region of the Atacama Desert. Global Planet. Change 185, 103090.
Mörchen, R., Lehndorff, E., Diaz, F.A., Moradi, G., Bol, R., Fuentes, B., Klumpp, E., Amelung, W., 2019. Carbon accrual in the Atacama Desert. Global Planet. Change 181, 102993.
Mörchen, R., Amelung, W., Giese, C., Böhnert, T., Ruhm, J., Lehndorff, E., 2021. Fingerprint of plant life in the Atacama Desert – Insights from *n*-alkane analyses. Org Geochem. 151, 104145.
Oerter, E., Amundson, R., Heimsath, A., Jungers, M., Chong, G., Renne, P., 2016. Early to middle Miocene climate in the Atacama Desert of Northern Chile. Palaeogeogr. Palaeoclimatol. Palaeoecol. 441 (4), 890–900.
Okin, G.S., Mahowald, N., Chadwick, O.A., Artaxo, P., 2004. Impact of desert dust on the biogeochemistry of phosphorus in terrestrial ecosystems. Global Biogeochem Cy. 18 (2), GB2005.
Orlando, J., Alfaro, M., Bravo, L., Guevara, R., Carú, M., 2010. Bacterial diversity and occurrence of ammonia-oxidizing bacteria in the Atacama Desert soil during a "desert bloom" event. Soil Biol. Biochem. 42 (7), 1183–1188.
Ortega, C., Vargas, G., Rojas, M., Rutllant, J.A., Muñoz, P., Lange, C.B., Pantoja, S., Dezileau, L., Ortlieb, L., 2019. Extreme ENSO-driven torrential rainfalls at the southern edge of the Atacama Desert during the Late Holocene and their projection into the 21th century. Global Planet. Change 175, 226–237.
Owen, J.J., Dietrich, W.E., Nishiizumi, K., Chong, G., Amundson, R., 2013. Zebra stripes in the Atacama Desert: Fossil evidence of overland flow. Geomorphology 182, 157–172.
Pfeiffer, M., Morgan, A., Heimsath, A., Jordan, T., Howard, A., Amundson, R., 2021. Century scale rainfall in the absolute Atacama Desert: landscape response and implications for past and future rainfall. Quaternary Sci. Rev. 254, 106797.
Placzek, C.J., Matmon, A., Granger, D.E., Quade, J., Niedermann, S., 2010. Evidence for active landscape evolution in the hyperarid Atacama from multiple terrestrial cosmogenic nuclides. Earth Planet. Sc. Lett. 295 (1-2), 12–20.
Quade, J., Rech, J.A., Latorre, C., Betancourt, J.L., Gleeson, E., Kalin, M.T.K., 2007. Soils at the hyperarid margin: The isotopic composition of soil carbonate from the Atacama Desert, Northern Chile. Geochim. Cosmochim. Ac. 71 (15), 3772–3795.
Rech, J.A., Quade, J., Hart, W.S., 2003. Isotopic evidence for the source of Ca and S in soil gypsum, anhydrite and calcite in the Atacama Desert. Chile. Geochim. Cosmochim. Ac. 67 (4), 575–586.
Rech, J.A., Currie, B.S., Michalski, G., Cowan, A.M., 2006. Neogene climate change and uplift in the Atacama Desert, Chile. Geology 34, 761–764.
Regelink, F., Weng, L., Lair, G.J., Comans, R.N., 2015. Adsorption of phosphate and organic matter on metal (hydr)oxides in arable and forest soil: a mechanistic modelling study. Eur. J. Soil Sci. 66 (5), 867–875.
Reyers, M., Hamidi, M., Shao, Y., 2019. Synoptic analysis and simulation of an unusual dust event over the Atacama Desert. Atmos. Sci. Lett. 20, 1–9.
Reyers, M., Boehm, C., Knarr, L., Shao, Y., Crewell, S., 2021. Synoptic-to-Regional-Scale analysis of rainfall in the Atacama Desert (18°–26°S) using a long-term simulation with WRF. Mon. Weather Rev. 149 (1), 91–112.
Riquelme, R., Martinod, J., Hérail, G., Darrozes, J., Charrier, R., 2003. A geomorphological approach to determining the Neogene to Recent tectonic deformation in the Coastal Cordillera of northern Chile (Atacama). Tectonophysics 361 (3–4), 255–275.
Ritter, B., Wennrich, V., Medialdea, A., Brill, D., King, G., Schneiderwind, S., Niemann, K., Fernández-Galego, E., Diederich, J., Rolf, C., Bao, R., Melles, M., Dunai, T.J., 2019. Climatic fluctuations in the hyperarid core of the Atacama Desert during the past 215 ka. Sci. Rep. 9, 5270.
Sáez, A., Cabrera, L., Garcés, M., Bogaard, P.V.D., Jensen, A., Gimeno, D., 2012. The stratigraphic record of changing hyperaridity in the Atacama desert over the last 10 Ma. Earth Planet. Sc. Lett. 355-356, 32–38.
Sager, C., Airo, A., Arens, F.L., Schulze-Makuch, D., 2021. New type of sand wedge polygons in the salt cemented soils of the hyper-arid Atacama Desert. Geomorphology 373, 107481.
Said-Pullicino, D., Giannetta, B., Demeglio, B., Missong, A., Gottselig, N., Romani, M., Bol, R., Klumpp, E., Celi, L., 2021. Redox-driven changes in water-dispersible colloids and their role in carbon cycling in hydromorphic soils. Geoderma 385, 114894.

Schween, J.H., Hoffmeister, D., Löhnert, U., 2020. Filling the Observational Gap in the Atacama Desert with a New Network of Climate Stations. Global Planet. Change 184, 103034.
Séquaris, J.M., Lewandowski, H., 2003. Physicochemical characterization of potential colloids from agricultural topsoils. Colloid. Surface. A 217 (1–3), 93–99.
Smedley, R.K., Duller, G.A.T., Pearce, N.J.G., Roberts, H.M., 2012. Determining the K-content of single-grains of feldspar for luminescence dating. Radiat. Meas. 47 (9), 790–796.
Sun, T., Bao, H., Reich, M., Hemming, R., 2018. More than ten million years of hyper-aridity recorded in the Atacama Gravels. Geochim. Cosmochim. Ac. 227, 123–132.
Totsche, K.U., Amelung, W., Gerzabek, M.H., Guggenberger, G., Klumpp, E., Knief, C., Lehndorff, E., Mikutta, R., Peth, S., Prechtel, A., Ray, N., Kögel-Knabner, I., 2018. Microaggregates in soils. J. Plant Nutr. Soil Sc. 181 (1), 104–136.
Walk, J., Stauch, G., Reyers, M., Vásquez, P., Sepúlveda, F.A., Bartz, M., Hoffmeister, D., Brückner, H., Lehmkuhl, F., 2020. Gradients in climate, geology, and topography affecting coastal alluvial fan morphodynamics in hyperarid regions-The Atacama perspective. Global Planet. Change 185, 102994.
Walk, J., Schulte, P., Bartz, M., Binnie, A., Kehl, M., Mörchen, R., Sun, X., Stauch, G., Tittmann, C., Bol, R., Brückner, H., Lehmkuhl, F., 2023. Pedogenesis at the coastal arid-hyperarid transition deduced from a Late Quaternary chronosequence at Paposo, Atacama Desert. Catena 228, 107171.
Wang, F., Michalski, G., Seo, J.H., Ge, W., 2014. Geochemical, isotopic, and mineralogical constraints on atmospheric deposition in the hyper-arid Atacama Desert, Chile. Geochim. Cosmochim. Ac. 135, 29–48.
Wang, L., Missong, A., Amelung, W., Willbold, S., Prietzel, J., Klumpp, E., 2020. Dissolved and colloidal phosphorus affect P cycling in calcareous forest soils. Geoderma 375, 114507.
Williams, R.M.E., Irwin, R.P., Noe Dobrea, E.Z., Howard, A.D., Dietrich, W.E., Cawley, J. C., 2021. Inverted channel variations identified on a distal portion of a bajada in the central Atacama Desert, Chile. Geomorphology 393, 107925.
Yan, J., Manelski, R., Vasilas, B., Jin, Y., 2018. Mobile colloidal organic carbon: An underestimated carbon pool in global carbon cycles? Front. Env. Sci. 6, 12.
Yang, X., Chen, X., Yang, X., 2019. Effect of organic matter on phosphorus adsorption and desorption in a black soil from Northeast China. Soil Tillage Res. 187, 85–91.
Zhang, Q., Bol, R., Amelung, W., Missong, A., Siemens, J., Mulder, I., Willbold, S., Müller, C., Westphal Muniz, A., Klumpp, E., 2021. Water dispersible colloids and related nutrient availability in Amazonian Terra Preta soils. Geoderma 397, 115103.